

Illusion Thermotics

Run Hu, Shuling Zhou, Ying Li, Dang-Yuan Lei, Xiaobing Luo,* and Cheng-Wei Qiu*

“Fata Morgana” or “Mirage” phenomena have long been captivated as optical illusions, which actually relies on gradient-density air or vapor. Man-made optical illusions have witnessed significant progress by resorting to artificially structured metamaterials. Nevertheless, two long-standing challenges remain formidable: first, exotic parameters (negative or less than unity) become inevitable; second, the signature of original object is altered to that of a virtual counterpart. It is thus not able to address the holy grail of illusion per se, since a single virtual object still exposes the location. In this study, those problems are successfully addressed in a particular setup—illusion thermotics, which identically mimics the exterior thermal behavior of an equivalent reference and splits the interior original heat source into many virtual signatures. A general paradigm to design thermal illusion metadevices is proposed to manipulate thermal conduction, and empower robust simultaneous functions of moving, shaping, rotating, and splitting heat sources of arbitrary cross sections. The temperature profile inside the thermal metadvice can mislead the awareness of the real location, shape, size, and number of the actual heat sources. The present concept may trigger unprecedented development in other physical fields to realize multiple functionalized illusions in optics, electromagnetics, etc.

Optical illusions, which people may refer to *Fata Morgana* or *Mirage*, are visually perceived images but deceptive and misleading. The essence of such illusions is attributed to the inhomogeneous density of air molecules, resulting in varying refraction index in air during light propagation. Analogously, an object of arbitrary shape, location, size, and material properties can also be identified by an infrared (IR) camera


as another one with different shape, location, size, or makeup, which is called as thermal illusions.^[1–6] Our mother nature offers countless animals, such as chameleons, stick insects, and some spiders, cuttlefish and octopuses, etc., which possess amazing color-changing capabilities to create optical/thermal illusions to camouflage themselves against the environment for disguise, protection, hunting, or species reproduction.^[7–9] Inspired by such illusion phenomena, man-made optical/thermal illusions have witnessed significant progress by resorting to artificially structured inhomogeneous metamaterials^[10–27] or metasurfaces,^[28,29] and the concept of illusion optics is proposed thereby.^[30,31] Nevertheless, two long-standing challenges remain formidable. On the one hand, they usually rely on negative or less-than-unity (the parameter of background considered as the reference unity) parameters that are hard to realize in nature.^[32–34] This issue is more challenging in thermal metamaterials since the nature forbids us to use negative thermal conductivities by the second law

of thermodynamics, which is distinguished from its optical counterpart.^[35–37] On the other hand, the traditional illusion operation is to alter the presence of the original heat source into that of a virtual counterpart in a different form. However, the virtual form is usually still one-to-one mapping, and thereby the illusion heat source still exposes the location though its shape could differ from the original one. As shown in **Figure 1a,b**, the state-of-the-art thermal illusion techniques^[1–3] only realize exactly the same exterior thermal signature as the reference (the red and blue curves overlap outside the device). Unfortunately, it is quite easy to locate the target with an infrared camera by searching the maximum temperature location inside the device, as shown in **Figure 1b**. Typical examples can be found in refs. [1–3]. The current illusion techniques could neither change the number of heat signatures nor realize both interior and exterior illusion simultaneously. Actually, neither the existing transformation thermotics nor transformation optics^[38–44] have been reported to solve such two problems simultaneously yet. However, can we solve both problems stated in the Abstract in order to achieve interior and exterior illusions at one go with positive parameters throughout? If we can realize multiple heat signatures inside the device while maintaining the existing illusion performance outside, as shown in **Figure 1c**, the target (say an object or an individual) can realize the function

Prof. R. Hu, S. L. Zhou, Prof. X. B. Luo
School of Energy and Power Engineering
Huazhong University of Science and Technology
Wuhan 430074, China
E-mail: luoxb@hust.edu.cn

Dr. Y. Li, Prof. C.-W. Qiu
Department of Electrical and Computer Engineering
National University of Singapore
Kent Ridge 117583, Republic of Singapore
E-mail: eleqc@nus.edu.sg

Prof. D.-Y. Lei
Department of Applied Physics
The Hong Kong Polytechnic University
Hung Hom, Hong Kong, China

 The ORCID identification number(s) for the author(s) of this article can be found under <https://doi.org/10.1002/adma.201707237>.

DOI: 10.1002/adma.201707237

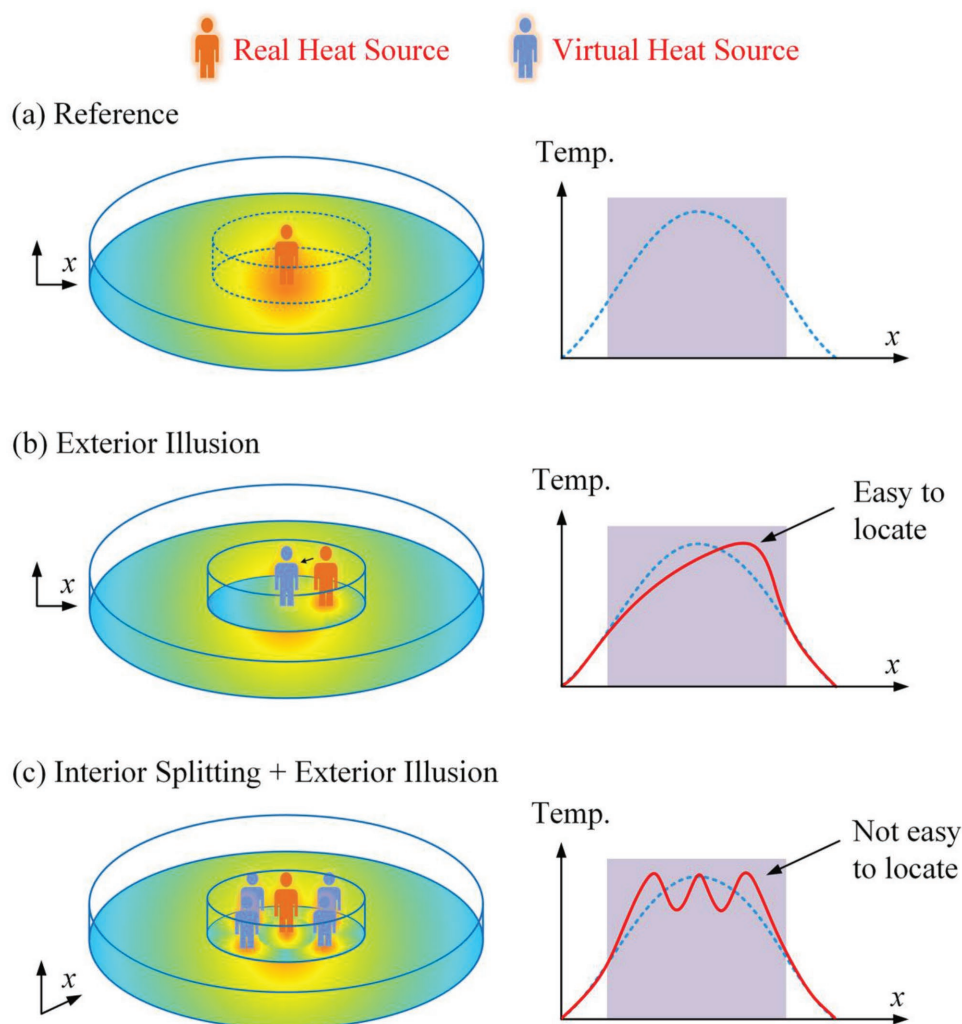


Figure 1. Schematic operation of illusion thermotics. a) Reference temperature. The signature shows a “red man” (the real heat source) at the center of the temperature field without an illusion device. b) Current practice of exterior illusion. In a conventional illusion device, the “red man” is expected to move to the location of the “blue man” (the virtual heat source) while maintaining the exterior temperature (red line and blue line overlap). From the exterior temperature, one may not be aware of the interior action of moving, which is the desired consequence for conventional illusion device. However, we may still observe the maximum temperature is at the “red man” and locate the target (maximum temperature) from the temperature field. c) Exterior illusion cum interior splitting. The “red man” is split into four and located at four different places while the exterior temperature is still maintained simultaneously (red line and blue line overlap). It then becomes difficult to locate the real target from the temperature curve compared with (b). The interior temperature will mislead us to locate the real target in terms of location, shape, rotation, and number. The shadow area denotes the device region.

of “Multi-location” or “Multi-Shadow Clone Jutsu,” i.e., the target illusions appear to be located at multiple distinct places at the same time. If so, it becomes not straightforward to locate the original heat source among several illusion signatures in Figure 1c and the deceptiveness will be enhanced greatly and unprecedentedly. This ultimate curiosity stimulates us to explore and develop a general paradigm to design such thermal illusion metadevices in this study. Detailed design processes were introduced and validated theoretically and experimentally.

As shown in **Figure 2**, our goal is to split the original target (rectangular $P_1'Q_1'Q_4'P_4'$) in the real space (x', y') into two illusion targets (rectangular $P_1Q_1M_1N_1$ and rectangular $P_4Q_4M_4N_4$) in the virtual space (x, y) with different shapes and orientations. The real space is divided into eight triangles denoted

by numbers 1' to 8', and the corresponding triangle regions in the virtual space are denoted by numbers 1–8. The two illusion targets in the right-hand space are rotated by θ_1 and θ_4 (for consistency with below context), respectively. According to the coordinate transformation relationship, each point (x, y) in each triangle region can then be mapped to new one (x', y') in the corresponding triangle by the following linear relationship as^[3]

$$\begin{bmatrix} x'_i \\ y'_i \\ 1 \end{bmatrix} = \begin{bmatrix} \alpha_i & \beta_i & \gamma_i \\ \mu_i & \nu_i & \varepsilon_i \\ 0 & 0 & 1 \end{bmatrix} \begin{bmatrix} x_i \\ y_i \\ 1 \end{bmatrix} \quad (1)$$

where $\alpha, \beta, \gamma, \mu, \nu$, and ε are the six undetermined coefficients, subscript index i ($= 1-8$) denotes the i th triangle section, and the superscript denotes the transformed space. Since we can

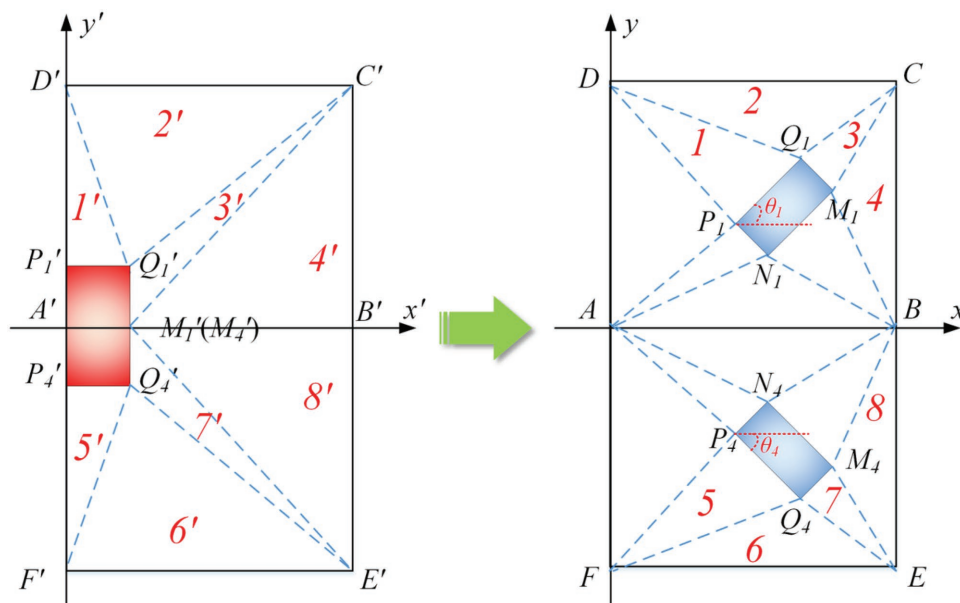


Figure 2. Schematic of the coordinate transformation for rectangular targets.

design the coordinates of the original and the moved targets, the six coefficients of each triangle can be easily obtained by substituting the three vertexes of each triangle into Equation (1), respectively. Note that Figure 2 just illustrates the transformation in the right-hand space of x -axis, and we can also extend it to the whole space as desired.

On the other hand, according to the Fourier's law of heat conduction, the heat flux in the i th direction (q_i) under a given temperature gradient in the j th direction (∇T_j) can be expressed as $q_i = -\kappa_{ij} \nabla T_j$, where $\kappa_{ij} = \begin{bmatrix} \kappa_{xx} & \kappa_{xy} \\ \kappa_{yx} & \kappa_{yy} \end{bmatrix}$ is the second-order thermal conductivity tensor of the materials. Based on the principle of the transformation thermotics, the Fourier equation maintains form invariant after coordinate transformation. In return, an adjustment arises on the thermal conductivity tensor from the virtual space (x, y) to the real space (x', y'), which can be expressed as^[22,44,45]

$$\kappa'_{ij} = \begin{bmatrix} \kappa'_{xx} & \kappa'_{xy} \\ \kappa'_{yx} & \kappa'_{yy} \end{bmatrix} = \frac{J_i \kappa_0 J_i^\dagger}{\det(J_i)} \quad (2)$$

where κ_0 is the homogeneous thermal conductivity in the virtual space and J_i is the Jacobian matrix of the coordinate transformation in i th triangle, as $J_i = \frac{\partial(x', y')}{\partial(x, y)} = \begin{bmatrix} \alpha_i & \beta_i \\ \mu_i & \nu_i \end{bmatrix}$, and J_i^\dagger is the transpose matrix of J_i . After substituting all the coefficients of each linear mapping relationship into Equation (2), we can obtain the required thermal conductivity tensor in the real space for each triangle region. To validate our general design method, we present four designs in series, i.e., (1) a symmetrical rectangular case with experimental verification, (2) two asymmetrical cases, and (3) a general case with arbitrary cross section.

In the first validation, both the original rectangular target and the split illusion ones are symmetric to the x and y -axes.

The dimensions of the original target are $10 \times 10 \text{ mm}^2$, and that of the illusion targets are $30 \times 5 \text{ mm}^2$ ($P_m Q_m \times P_m N_m$), where the subscript m ($= 1, 2, 3, 4$) denotes the four quadrants in the x - y plane. The rotation angles θ_m of the four illusion targets are the same as 5° with respect to the x -axis. The dimensions of the illusion device are $120 \times 100 \text{ mm}^2$. The coordinates of points P_m are (25, 20), (−25, 20), (−25, −20), and (25, −20) mm, respectively. In the experiments, we fabricated two prototypes by a $200 \times 160 \text{ mm}^2$ copper plate with uniformly filled holes with radius $r = 1.5 \text{ mm}$ and pitch $p = 5 \text{ mm}$. Therefore the effective thermal conductivity of the background plate can be calculated as $\kappa_0 = (1 - \pi r^2/p^2) \kappa_{Cu}$, which is designed to be consistent with the reference thermal conductivity in the illusion device region as shown in Table 1. The required thermal conductivity κ' for each triangle region can be calculated according to Equation (2), and those in the first quadrant are listed in Table 1. These thermal conductivity tensors are all symmetric matrix, i.e.,

satisfying $\kappa' = \kappa'^T = \begin{bmatrix} \kappa'_{xx} & \kappa'_{xy} \\ \kappa'_{yx} & \kappa'_{yy} \end{bmatrix}$, so they can be diagonalized

into $\begin{bmatrix} \kappa'_x & 0 \\ 0 & \kappa'_y \end{bmatrix}$, where $\kappa'_{x,y} = (\kappa'_{xx} + \kappa'_{yy} \pm \sqrt{(\kappa'_{xx} - \kappa'_{yy})^2 + 4\kappa'^2_{xy}})/2$,

and the rotation angle θ of the matrix is $\theta = 0.5 \tan^{-1}[2\kappa'_{xy}/(\kappa'_{xx} - \kappa'_{yy})]$.^[24,44] Further, we can apply the effective medium

theory to realize $\begin{bmatrix} \kappa'_x & 0 \\ 0 & \kappa'_y \end{bmatrix}$ by two rotated layered isotropic

materials A and B. The thermal conductivity of materials A and B can be calculated as $\kappa_{A,B} = \kappa'_x \pm \sqrt{\kappa'^2_x - \kappa'_x \kappa'_y}$ if the layer thickness is uniform.^[20,24] The specific material details in the first quadrant are listed in Table 1 as well and those in other quadrants can be easily obtained due to the symmetry.

With κ' or κ_A and κ_B , we can realize the desired thermal illusion in theory, but sometimes it is difficult to find/fabricate such materials. To solve this, we drilled copper plates in device region with paralleled stripes/holes with corresponding orientations by laser carving process on a CNC machine, as shown

Table 1. Material details of each triangle in the first quadrant.

Region	1'	2'	3'	4'
κ'/κ_0	$\begin{bmatrix} 0.176 & 0.695 \\ 0.695 & 8.420 \end{bmatrix}$	$\begin{bmatrix} 2.628 & 1.822 \\ 1.822 & 1.643 \end{bmatrix}$	$\begin{bmatrix} 7.352 & 2.428 \\ 2.428 & 0.938 \end{bmatrix}$	$\begin{bmatrix} 11.756 & 3.769 \\ 3.769 & 1.294 \end{bmatrix}$
$\begin{bmatrix} \kappa'_x & 0 \\ 0 & \kappa'_y \end{bmatrix}/\kappa_0$	$\begin{bmatrix} 8.479 & 0 \\ 0 & 0.118 \end{bmatrix}$	$\begin{bmatrix} 4.023 & 0 \\ 0 & 0.249 \end{bmatrix}$	$\begin{bmatrix} 8.167 & 0 \\ 0 & 0.122 \end{bmatrix}$	$\begin{bmatrix} 12.973 & 0 \\ 0 & 0.077 \end{bmatrix}$
κ_A/κ_0	16.9	7.92	16.27	25.91
κ_B/κ_0	0.06	0.13	0.06	0.04
Θ	85.21°	37.44°	18.57°	17.89°
F	44%	74%	46%	14%
$\kappa_f^{a)}$	1.37	4.92	1.49	0.28

^{a)}Unit: W m⁻¹ K⁻¹.

in **Figure 3a–c**. The strips/holes are filled with low- κ materials to realize the required anisotropic thermal characteristics equivalently. The effective thermal conductivity tensor is $\begin{bmatrix} \kappa'_x & 0 \\ 0 & \kappa'_y \end{bmatrix}$, where the diagonal components $\kappa'_x = f\kappa_f + (1-f)\kappa_{Cu}$ and $\kappa'_y = (f/\kappa_f + (1-f)/\kappa_{Cu})^{-1}$ with f being the filling ratio of the stripes/holes and κ_f the thermal conductivity of the filling materials. By making the calculated thermal conductivity tensors equivalent to the experimental filling ones, we obtained the filling ratio f and the filling materials κ_f of the illusion devices at each triangle, as listed in Table 1. The filling materials were synthesized by mixing ≈ 6 μ m hexagonal boron nitride (hBN) particles (AC-6041, Momentive) with epoxy and calibrated with Laser Flash Analyzer (LFA 467) according to the required κ_f . Due to the color of the epoxy-based mixture, the filled holes/strips in the illusion device region look white, whose orientation and filling materials are consistent with θ and κ_f , and the thickness of the stripes/holes is determined by the filling ratio f . An IR camera (FLIR SC620) was used to observe the distribution of temperature fields and the emissivity was set as 0.98. The ambient temperature was 25 °C. Besides experiments, we also did finite-element simulations for the devices with the same dimensions, materials, and boundary conditions as the experiments except for the neglecting of air convection. For comparison, the illusion temperature with four illusion heat sources was also measured and simulated.

The experimental and simulated temperature fields of the first validation are shown in Figure 3d–i. The temperature curves along the large dashed circle in Figure 3h,i with radius of 80 mm are shown in Figure 3j. The red curve overlaps with the blue one well, which implies excellent exterior illusion. The exterior illusion could also be observed when comparing the two temperature fields with the device and of the illusion in both simulations and experiments. It is seen that the temperature contours are similar to each other outside the device region, which is the exact outcome of exterior thermal illusion that we cannot detect what is happening inside the device from the outside. The temperature curves along the small dashed circles in Figure 3h,i with constant radius of 30 mm are shown in Figure 3k. The four local temperature peaks along the red curve indicate that, except for the original heat source in the center,

four additional illusion heat sources emerge within the illusion devices, just like the four peaks along the blue curve corresponding to four separated illusion heat sources in Figure 3i. It seems as if the real heat source is split into four at different locations simultaneously. Together with the original heat source, the “five” heat sources will increase the deceptiveness. Therefore, judging from the temperature fields in the IR vision, the exterior temperature cannot tell us what is happening inside, and the interior temperature may lead us to wrongly assume that the heat sources are located at somewhere away from the original one and the number of heat sources is 4 rather than 1 in the center. By such “interior splitting + exterior illusion,” both the interior and exterior temperature will confuse us, which enhances the deceptiveness greatly and is the predominant advantage over the previous thermal illusions. From Figure 3, it is validated that (1) the target is moved to somewhere else off its original location; (2) the shape of the target is changed; (3) the target is rotated by a predesigned angle; and (4) the one target is split into four. Experimental results also show the “inner splitting + exterior illusion,” which may be not as perfect as those in the simulations since the thermal conductivity of the fabricated devices is not as anisotropic as those in theory and the natural convection is ignored in the simulation. From Figure 3, we can see that the outside temperature profiles are the same/similar, and the real heat source is split into multiple illusions inside the device. Since we only realize inner splitting rather than inner camouflage, the temperature profile discrepancy between Figure 3d,f inside the device or between the red and blue curves in Figure 3k can be attributed to the fact that we do not really move/split heat source, but only create split illusions. Thus the only heat source is still located in the center, and heat is conducted from the center to the ambient. Though we do not change the diffusive nature of heat conduction, which gives rise to the continuous temperature gradient between the real heat source and the illusion ones, the temperature of the split illusions can be as equivalent/close as that of the real heat source by present illusion thermotics. Such limitations may be removed by the counterpart physical fields, like optics. While in the reference experiment, there are four separated heat sources, thus we can observe four obvious hot spots in Figure 3f,i. Even though, we can still observe the split

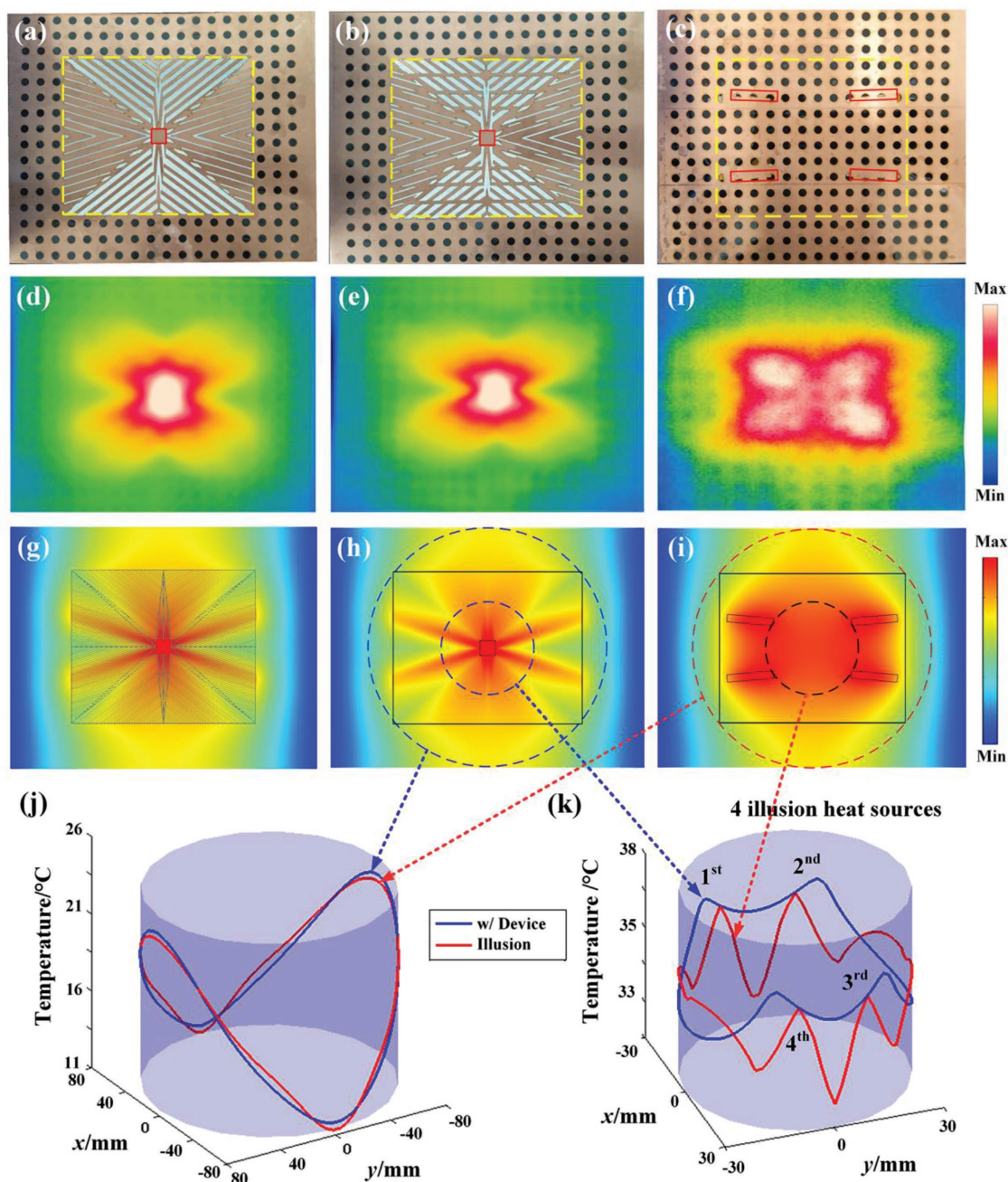


Figure 3. a,b) Two experimental prototypes and c) reference one. The red rectangles denote the heat source and the yellow dashed rectangles denote the region of the illusion devices. Experimental temperature fields of: d,e) the two prototypes and f) the referenced one. g) Simulated temperature fields with homogeneous layered structures of κ_A and κ_B . Simulated temperature fields with illusion device with: h) inhomogeneous κ' and i) the reference one. j) Temperature curves along the large dashed circle in (h) and (i) with constant distance away from the heat source of 80 mm. Good agreement of the two curves implies excellent “exterior illusion.” k) Temperature curves along the small dashed circle in (h) and (i) with constant distance of 30 mm. Four local temperature peaks indicate four splitting illusion/equivalent heat sources. Clear “interior splitting + exterior illusion” performances are observed.

illusions in Figure 3g,h,k. Such improvement not only verifies the shortage of the conventional design but also enhances the deceptiveness in the present design. The proposed device identically mimics the exterior thermal behavior of an equivalent reference and splits the interior original heat source into many virtual signatures, which will mislead the awareness of the real

location, shape, and number of the actual heat sources. Moreover, the target can also be split into two, three, four, or even more with small modifications to the present design method. For instance, when two of the split sub-sources contact/overlap with each other, the original heat source seems to be split into two or three (see Figure 4a). The current splitting of space is

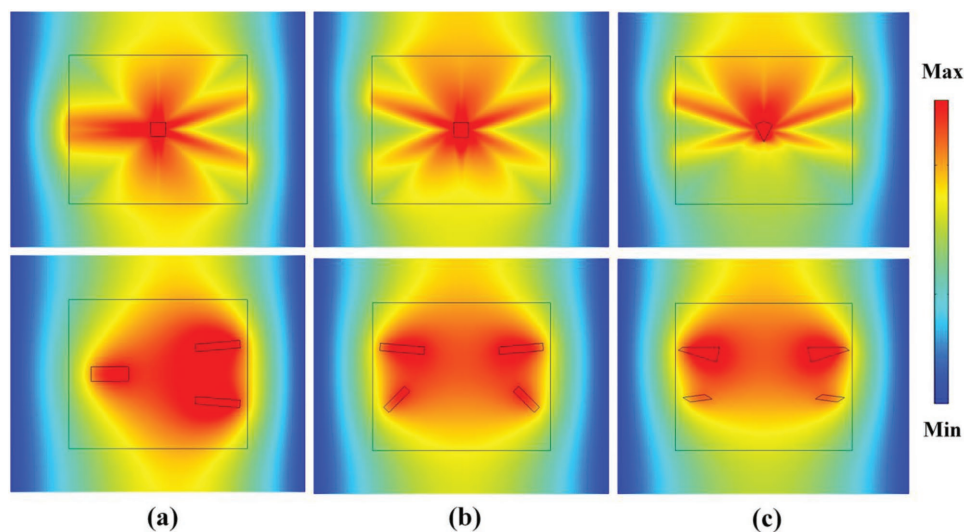


Figure 4. Temperature profile with the illusion device and illusion temperature for: a) asymmetrical case with three illusions, b) asymmetrical rectangular targets, and c) arbitrary targets. Clear “interior splitting + exterior illusion” performances are observed in all the cases.

orthogonal/polygonal, while it can also be extended into radial one with multiple triangle-shape or sensu-shape sub-regions, then the flexibility and applicability will be greatly enhanced. Further, we may extend the present 2D design into 3D case with more degrees of freedom. Figure 3 is the exact expectation of our design and the thermal illusion is achieved satisfyingly with increased deceptiveness.

In the second and the third validation, the illusion targets are asymmetric to the x -axis. In the second one, the coordinates for points P_1 and P_4 are (25, 20) mm and (35, -10) mm, respectively. The dimensions for the two rectangular illusion targets are $30 \times 5 \text{ mm}^2$ ($P_1Q_1 \times P_1N_1$) and $20 \times 5 \text{ mm}^2$ ($P_4Q_4 \times P_4N_4$). The rotation angles θ_1 and θ_4 are 5° and 45° , respectively. In the third validation, as shown in Figure 5, the original target is

an arbitrary triangle with coordinates of $P_1'(0, 6)$, $Q_1'(6, 4)$, and $Q_4'(0, -8)$ mm, respectively. The illusion targets are arbitrary convex quadrangles with coordinates of $P_1(30, 20)$, $Q_1(55, 20)$, $M_1(58, 18)$, $N_1(32, 10)$, $P_4(35, -15)$, $Q_4(50, -17)$, $M_4(55, -14)$, and $N_4(40, -12)$ mm, respectively. Other parameters are maintained the same. The simulated temperature fields of the second and third validations are shown in Figure 4b,c. It is seen that since the illusion targets are asymmetric, the temperature profile in each case is not symmetric accordingly. Nevertheless, the device can still split the original heat source into multiple asymmetric illusions at different locations. The temperature fields with the device and the illusion show similar exterior temperature contours and multiple-location illusion heat sources inside. Here we do not repeat the similar discussion as those about Figure 3

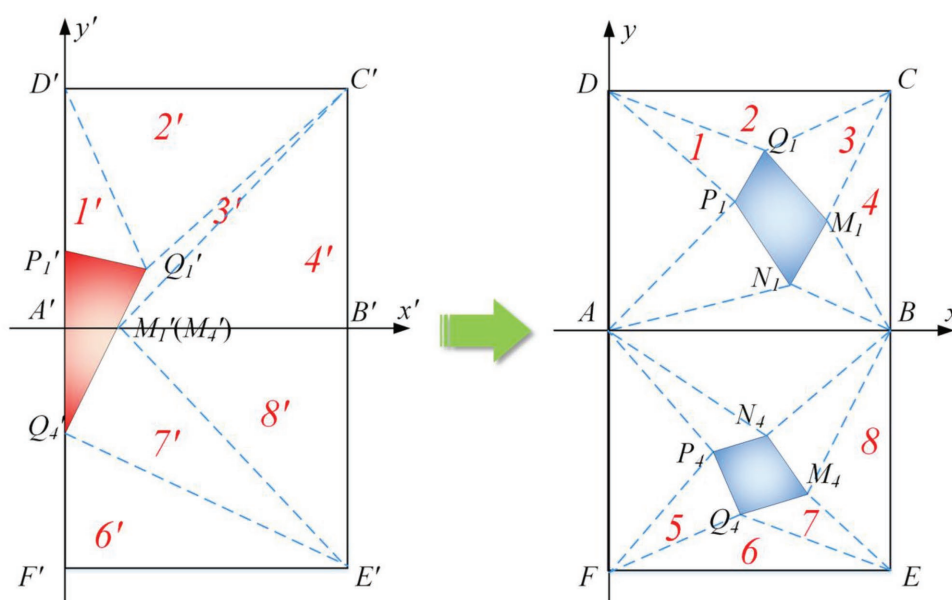


Figure 5. Schematic for the coordinate transformation for arbitrary targets.

as a similar “interior splitting + exterior illusion” function of the asymmetric design is also achieved, which substantially proves that our design method can be applied for asymmetric cases and arbitrary cross-section targets satisfyingly as well. What is more, the original target is a triangle in Figure 4c, yet with their four illusions being quadrangles, which implies that the vertex number of illusions can be adjusted and the present method is flexible for arbitrary polygonal illusion.

In summary, we propose a general paradigm to design illusion devices to manipulate heat conduction and empower robust simultaneous function of moving, shaping, rotating, and splitting targets with arbitrary cross section. Based on the paradigm, symmetric, asymmetric, and arbitrary cross section cases are presented theoretically and experimentally, demonstrating the outcome that the interior region of the original heat source is thereby split and camouflaged, while the exterior thermal signature is remained the same as the reference. The original heat source can be hidden among several illusion heat sources, and such interesting function is somewhat similar to the *Multi-location* ability in the fairy tales or fictions. Such “interior splitting + exterior illusion” effect can mislead the awareness of the right location, shape, and number of the actual heat sources, enhancing the deceptiveness greatly in an unprecedented manner. We achieve a very high-caliber illusion thermotics, even in the environment where negative parameters (conductivity) are not present. The present method and devices may open avenues for the flexible design, feasible fabrication, and practical application of thermal illusion and thermal camouflage. It is true that heat is diffusive from the real heat source to the surroundings, thus we cannot really change the number and location of maxima in the temperature field, but we can realize the temperature of the illusion heat sources as equivalent/close as the real heat source, which seems as if the real heat source is split and multi-located at different places at the same time. The present concept can trigger unprecedented development in other physical fields to realize multiple functionalized illusions in optics, electromagnetics, acoustics, mechanics, etc.

Experimental Section

According to the theoretical designs, a $200 \times 160 \text{ mm}^2$ copper plate was drilled on with uniform holes with radius $r = 1.5 \text{ mm}$ and pitch $p = 5 \text{ mm}$ outside the rectangular illusion region, and predesigned rectangular stripes/holes were drilled inside the illusion region. The size of the rectangular stripes/holes was determined by the calculated filling ratio f and their orientations are θ , as shown in Table 1. Note that the information in Table 1 is just the first quadrant and those in other quadrants can be easily obtained with symmetry considerations. The copper plate possesses two 25 cm long feet perpendicular to the plate at the two ends for water bath. According to filling material κ_f in the rectangular hole in the illusion region, the hBN particles (AC-6041, Momentive) were mixed with epoxy matrix. The lateral size of the hBN particle is $\approx 6 \mu\text{m}$, and the thickness is $\approx 0.1\text{--}0.5 \mu\text{m}$. The in-plane and out-of-plane thermal conductivity is >300 and $\approx 3 \text{ W m}^{-1} \text{ K}^{-1}$, respectively. After stirring the mixture for $>20 \text{ min}$, the mixture was put in a vacuum pump to expel the air bubble for $>2 \text{ h}$. The thermal conductivity of the mixture was measured and calibrated with a Laser Flash Analyzer (LFA 467) according to the required κ_f in each triangle of the illusion region. Then the front side of the copper plate was wrapped with a transparent adhesive tape and the reason for doing this is twofold. One

is to help the filling process of the hBN–epoxy mixture, and the other is to maintain the same emissivity throughout the infrared imaging. The copper plate was put upside down on an electrical heater and the rectangular hole was filled in the illusion region with corresponding mixtures. The circular holes were not filled and remained empty. After filling, the mixture was cured for 2 h on the electrical heater at 80°C . Then two water-bath containers were prepared at the two sides of the copper plate. The size of the container was 40 cm long, 30 cm wide, and 30 cm high. The container was first filled with room-temperature water for $1/3$ volume and then enough ice was added to $2/3$ volume. A mercurial thermometer was used to measure the water temperature. If the water temperature was above zero, some ice was added in time to maintain the water temperature at 0°C . An IR camera (FLIR SC620) was used to observe the temperature fields and the emissivity was set as 0.98 with calibration by thermocouple. The distance between the copper plate and the IR camera was $\approx 0.7 \text{ m}$, and the camera was finely zoomed to make the image clear. Two kinds of ceramic heaters were used in the experiments and set at the back side of the copper plate: a square-shape one with a dimension of $10 \times 10 \text{ mm}^2$ was used to heat up the proposed device and a rectangular one with a dimension of $30 \times 5 \text{ mm}^2$ was used in the reference experiment. The copper plates were maintained horizontally and the left and right feet were immersed in the mixture of ice and water. The room temperature was kept at 25°C .

Acknowledgements

The authors would like to acknowledge the financial support from the National Natural Science Foundation of China (Grant Nos. 51606074 and 51625601), the National Key Research and Development Program of China (Project Nos. 2016YFB0100901 and 2016YFB0400804), and the Ministry of Science and Technology of the People's Republic of China (Project No. 2017YFE0100600). C.-W.Q. acknowledges the financial support from the Ministry of Education, Singapore (Project No. R-263-000-C05-112). D.-Y.L. acknowledges the financial support from the National Natural Science Foundation of China (Grant No. 11474240).

Conflict of Interest

The authors declare no conflict of interest.

Keywords

coordinate transformation, splitting signatures, thermal camouflage, thermal illusion

Received: December 12, 2017

Revised: February 7, 2018

Published online: April 17, 2018

- [1] T. C. Han, X. Bai, J. T. L. Thong, B. W. Li, C. W. Qiu, *Adv. Mater.* **2014**, 26, 1731.
- [2] X. He, L. Z. Wu, *Appl. Phys. Lett.* **2014**, 105, 221904.
- [3] Q. W. Hou, X. P. Zhao, T. Meng, C. L. Liu, *Appl. Phys. Lett.* **2016**, 109, 103506.
- [4] N. Q. Zhu, X. Y. Shen, J. P. Huang, *AIP Adv.* **2015**, 5, 053401.
- [5] T. Z. Yang, Y. S. Su, W. K. Xu, X. D. Yang, *Appl. Phys. Lett.* **2016**, 109, 121905.
- [6] T. Z. Yang, X. Bai, D. L. Gao, L. Z. Wu, B. W. Li, J. T. L. Thong, C. W. Qiu, *Adv. Mater.* **2015**, 27, 7752.
- [7] S. A. Morin, R. F. Shepherd, S. W. Kwok, A. A. Stokes, A. Nemiroski, G. M. Whitesides, *Science* **2012**, 337, 828.
- [8] H. Yuk, S. T. Lin, C. Ma, M. Takaffoli, N. X. Fang, X. H. Zhao, *Nat. Commun.* **2017**, 8, 14230.

- [9] J. Teyssier, S. V. Saenko, D. Marel, M. C. Milinkovitch, *Nat. Commun.* **2015**, 6, 6368.
- [10] M. Maldovan, *Nature* **2013**, 503, 209.
- [11] M. Moccia, G. Castaldi, S. Savo, Y. Sato, V. Galdi, *Phys. Rev. X* **2014**, 4, 021025.
- [12] R. Schittny, M. Kadic, S. Guenneau, M. Wegener, *Phys. Rev. Lett.* **2013**, 110, 195901.
- [13] H. Y. Xu, X. H. Shi, F. Gao, H. D. Sun, B. L. Zhang, *Phys. Rev. Lett.* **2014**, 112, 054301.
- [14] Y. M. Zhang, H. Y. Xu, B. L. Zhang, *AIP Adv.* **2015**, 5, 053402.
- [15] M. Farhat, P. Y. Chen, H. Bagci, C. Amra, S. Guenneau, A. Alu, *Sci. Rep.* **2015**, 5, 9876.
- [16] R. Hu, B. Xie, J. Y. Hu, Q. Chen, X. B. Luo, *EPL* **2015**, 111, 54003.
- [17] Y. G. Ma, L. Lan, W. Jiang, F. Sun, S. L. He, *NPG Asia Mater.* **2013**, 5, e73.
- [18] X. He, L. Z. Wu, *Appl. Phys. Lett.* **2013**, 102, 211912.
- [19] E. M. Dede, T. Nomura, P. Schmalenberg, J. S. Lee, *Appl. Phys. Lett.* **2013**, 103, 063501.
- [20] R. Hu, X. L. Wei, J. Y. Hu, X. B. Luo, *Sci. Rep.* **2014**, 4, 3600.
- [21] S. Guenneau, C. Amra, *Opt. Express* **2013**, 21, 6578.
- [22] S. Narayana, Y. Sato, *Phys. Rev. Lett.* **2012**, 108, 214303.
- [23] Y. Li, X. Y. Shen, Z. H. Wu, J. Y. Huang, Y. X. Chen, Y. S. Ni, J. P. Huang, *Phys. Rev. Lett.* **2015**, 115, 195503.
- [24] R. Hu, S. L. Zhou, W. C. Shu, B. Xie, Y. P. Ma, X. B. Luo, *AIP Adv.* **2016**, 6, 125111.
- [25] S. Guenneau, D. Petiteau, M. Zerrad, C. Amra, T. Puvirajesinghe, *AIP Adv.* **2015**, 5, 053404.
- [26] A. V. Kildishev, E. E. Narimanov, *Opt. Lett.* **2007**, 32, 3432.
- [27] J. Luo, Y. Yang, Z. Yao, W. Lu, B. Hou, Z. H. Hang, C. T. Chan, Y. Lai, *Phys. Rev. Lett.* **2016**, 117, 223901.
- [28] H. C. Liu, B. Yang, Q. H. Guo, J. Shi, C. Guan, G. Zheng, H. Mühlenbernd, G. Li, T. Zentgraf, S. Zhang, *Sci. Adv.* **2017**, 3, e1701477.
- [29] N. I. Zhuludev, Y. S. Kivshar, *Nat. Mater.* **2012**, 11, 917.
- [30] Y. Lai, J. Ng, H. Y. Chen, D. Z. Han, J. J. Xiao, Z. Q. Zhang, C. T. Chan, *Phys. Rev. Lett.* **2009**, 102, 253902.
- [31] Y. Lai, J. Ng, H. Chen, Z. Zhang, C. T. Chan, *Front. Phys. China* **2010**, 5, 308.
- [32] Y. Lai, H. Zheng, Z. Q. Zhang, C. T. Chan, *J. Opt.* **2011**, 23, 024009.
- [33] J. Luo, W. Lu, Z. Hang, H. Chen, B. Hou, Y. Lai, C. T. Chan, *Phys. Rev. Lett.* **2014**, 112, 073903.
- [34] S. Palomba, S. Zhang, Y. Park, G. Bartal, X. B. Yin, X. Zhang, *Nat. Mater.* **2012**, 11, 34.
- [35] Y. Gao, J. P. Huang, Y. M. Liu, L. Gao, K. W. Yu, X. Zhang, *Phys. Rev. Lett.* **2010**, 104, 034501.
- [36] R. Hu, S. Zhou, X. Yu, X. B. Luo, *J. Phys. D: Appl. Phys.* **2016**, 49, 415302.
- [37] R. Hu, J. Hu, R. Wu, B. Xie, X. Yu, X. B. Luo, *Chin. Phys. Lett.* **2016**, 33, 044401.
- [38] W. X. Jiang, C. W. Qiu, T. C. Han, S. Zhang, T. J. Cui, *Adv. Funct. Mater.* **2013**, 23, 4028.
- [39] X. F. Zhu, L. Feng, P. Zhang, X. B. Yin, X. Zhang, *Opt. Lett.* **2013**, 38, 2821.
- [40] F. Sun, S. He, *Sci. Rep.* **2016**, 6, 19130.
- [41] C. Li, X. Meng, X. Liu, F. Li, G. Fang, H. Chen, C. T. Chan, *Phys. Rev. Lett.* **2010**, 105, 233906.
- [42] W. X. Jiang, T. J. Cui, *Opt. Express* **2010**, 18, 5161.
- [43] W. X. Jiang, T. J. Cui, X. M. Yang, H. F. Ma, Q. Cheng, *Appl. Phys. Lett.* **2011**, 98, 204101.
- [44] S. Guenneau, C. Amra, D. Veynante, *Opt. Express* **2012**, 20, 8207.
- [45] C. Z. Fan, Y. Gao, J. P. Huang, *Appl. Phys. Lett.* **2008**, 92, 251907.